

Doping induced metal-insulator transition in two-dimensional Hubbard, $t - U$, and extended Hubbard, $t - U - W$, models.

F.F. Assaad¹ and M. Imada²

¹ Institut für Theoretische Physik III,
Universität Stuttgart, Pfaffenwaldring 57, D-70550 Stuttgart, Germany.

² Institute for Solid State Physics, University of Tokyo,
7-22-1 Roppongi, Minato-ku, Tokyo 106, Japan.

Abstract

We show numerically that the nature of the doping induced metal-insulator transition in the two-dimensional Hubbard model is radically altered by the inclusion of a term, W , which depends upon a square of a single-particle nearest-neighbor hopping. This result is reached by computing the localization length, ξ_l , in the insulating state. At finite values of W we find results consistent with $\xi_l \sim |\mu - \mu_c|^{-1/2}$ where μ_c is the critical chemical potential. In contrast, $\xi_l \sim |\mu - \mu_c|^{-1/4}$ for the Hubbard model. At finite values of W , the presented numerical results imply that doping the antiferromagnetic Mott insulator leads to a $d_{x^2-y^2}$ superconductor.

PACS numbers: 71.27.+a, 71.30.+h, 71.10.+x

I. INTRODUCTION

The doping induced metal-insulator transition in the two-dimensional Hubbard model is anomalous in the sense that it cannot be understood in terms of a generic band metal-insulator transition [1–3]. This statement follows from numerical work at zero- and finite-temperatures on lattice sizes up to 16×16 . Zero-temperature quantum Monte-Carlo (QMC) calculations of the charge susceptibility, $\chi_c = \partial n / \partial \mu$, have shown that it behaves as $\chi_c \sim |\mu - \mu_c|^{-1/2}$ in the vicinity of the critical chemical potential μ_c at which the transition occurs [4]. This result is consistent with $t - J$ model calculations [5,6]. In principle, the square root singularity in χ_c can be reproduced within a mean-field spin density wave (SDW) approximation provided that perfect nesting is present and that antiferromagnetic order is retained upon shifting the chemical potential in the rigid band. When perfect nesting is absent the SDW approximation yields, as in the case of the generic band metal insulator transition, a chemical potential independent charge susceptibility. This stands in contrast to QMC results, which for a *small* violation of perfect nesting still show a square root singularity in χ_c as the critical chemical potential is approached [4]. The second piece of information signaling the anomalous nature of the metal insulator transition, is obtained via the numerical calculation of the localization length, ξ_l , in the insulating state. For the two-dimensional Hubbard model one obtains $\xi_l \sim |\mu - \mu_c|^{-1/4}$ [7]. In contrast the SDW approximation as well as the generic band metal-insulator transition yield a square root

singularity for ξ_l . Finally, a QMC calculation of the high frequency Hall coefficient, shows no divergence of this quantity in the vicinity of the metal-insulator transition [8]. As opposed to the case of the generic band metal insulator transition, it's magnitude remains small.

In a single-particle picture, those numerical observations may be understood by the occurrence of flat *bands* around the $(\pm\pi, 0)$, $(0, \pm\pi)$ points in the Brillouin zone. More precisely, at the critical chemical potential, the exponent obtained numerically from the localization length, ξ_l , imposes a $|\vec{k}|^4$ dispersion relation around those points. This flat dispersion relation required for the understanding of numerical data, has important implications. It must originate from a large wavenumber dependent renormalization of the charge excitations due to correlation effects since the ordinary van-Hove singularity does not generate such a pronounced flatness. Because of this flatness around the $(\pm\pi, 0)$ and $(0, \pm\pi)$ points, doped holes predominantly occupy those regions. Thus, at low doping the the regions around the $(\pm\pi, 0)$ and $(0, \pm\pi)$ points in the Brillouin zone govern the low energy physics. Such strong wavenumber dependent renormalization may in part be caused by strong scattering of the quasiparticle between $(\pi, 0)$ and $(0, \pi)$ by the antiferromagnetic fluctuation carrying momentum transfer (π, π) [9] as well as by Umklapp scattering [10]. The flat dispersion thus generated further enhances this scattering channel in a consistent fashion. The experimental observation of flat bands, in high- T_c cuprates is documented in [11–13].

The occurrence of flat bands suppresses the kinetic energy in the metallic state close to the metal-insulator transition. This places the metallic state as well as the nature of the metal-insulator transition close to potential instabilities. In this article, we show that the inclusion of a term W which depends upon the square of a nearest neighbor hopping changes radically the above described properties of the metal-insulator transition. We argue that the low energy physics of the added term, W , is partially contained in the three site terms [15] obtained in a strong coupling expansion (second order perturbation in the hopping) of the Hubbard model.

Our starting point is the Hubbard model on a square lattice:

$$H_{tU} = -\frac{t}{2} \sum_{\vec{i}} K_{\vec{i}} + U \sum_{\vec{i}} (n_{\vec{i},\uparrow} - \frac{1}{2})(n_{\vec{i},\downarrow} - \frac{1}{2}) \quad (1)$$

with the hopping kinetic energy

$$K_{\vec{i}} = \sum_{\sigma, \vec{\delta}} \left(c_{\vec{i},\sigma}^\dagger c_{\vec{i}+\vec{\delta},\sigma} + c_{\vec{i}+\vec{\delta},\sigma}^\dagger c_{\vec{i},\sigma} \right). \quad (2)$$

Here, $c_{\vec{i},\sigma}^\dagger$ ($c_{\vec{i},\sigma}$) creates (annihilates) an electron with z -component of spin σ on site \vec{i} , $n_{\vec{i},\sigma} = c_{\vec{i},\sigma}^\dagger c_{\vec{i},\sigma}$, and $\vec{\delta} = \pm\vec{a}_x, \pm\vec{a}_y$ where \vec{a}_x, \vec{a}_y are the lattice constants. The energy will be measured in units of t . The interaction we add, is given by:

$$H_W = -W \sum_{\vec{i}} K_{\vec{i}}^2. \quad (3)$$

One motivation of considering this form is that at half-band filling ($\mu = 0$) the Hamiltonian:

$$H_{tUW} = H_{tU} + H_W \quad (4)$$

is particle-hole invariant, and the W -term has a simple Hubbard Stratonovitch transformation. This has for important consequence that the sign problem may be avoided in QMC approaches at half-filling. The added W -term may have various origins, as pointed out in Ref. [14]. One possible route is to consider the nature of the metallic state near the Mott transition described above. The Mott insulating state itself is characterized by the irrelevance of single-particle processes due to the opening of a quasiparticle gap. In the insulating state, the occurrence of long-range antiferromagnetic order shows the relevance of two-particle processes in the particle-hole channel. In two-dimensions, the flatness of the charge excitations at small doping suppress the relevance of single-particle processes and enhances the importance of two-particle processes. In contrast to the Mott insulating state, particle-particle processes now contribute to the two-particle channel. The form H_W contains such generic terms of two-particle processes.

Here, we show the relationship between the W -term and the three site terms obtained in a strong coupling expansion of the Hubbard model. The W -term may be written as

$$H_W = H_W^{(1)} + H_W^{(2)} + H_W^{(3)} + H_W^{(4)} \quad (5)$$

with

$$H_W^{(1)} = -8WN \quad (6)$$

where N denotes the number of sites.

$$H_W^{(2)} = -W \sum_{\vec{i}, \sigma, \vec{\delta}, \vec{\delta}'} \left(c_{i, \sigma}^\dagger c_{i, -\sigma}^\dagger c_{i+\vec{\delta}', -\sigma} c_{i+\vec{\delta}, \sigma} + \text{H.c.} \right) \quad (7)$$

$$H_W^{(3)} = +W \sum_{\vec{i}, \vec{\delta}, \vec{\delta}', m=-1, 0, 1} \left(T_{i, \delta', m}^\dagger T_{i, \delta, m} + T_{i, \delta', m} T_{i, \delta, m}^\dagger \right) \quad (8)$$

and

$$H_W^{(4)} = -W \sum_{\vec{i}, \vec{\delta}, \vec{\delta}'} \left(\Delta_{i, \delta'}^\dagger \Delta_{i, \delta} + \Delta_{i, \delta'} \Delta_{i, \delta}^\dagger \right). \quad (9)$$

Here, $T_{i, \delta, 1}^\dagger = c_{i, \uparrow}^\dagger c_{i+\vec{\delta}, \uparrow}^\dagger$, $T_{i, \delta, -1}^\dagger = c_{i, \downarrow}^\dagger c_{i+\vec{\delta}, \downarrow}^\dagger$, $T_{i, \delta, 0}^\dagger = \left(c_{i, \uparrow}^\dagger c_{i+\vec{\delta}, \downarrow}^\dagger + c_{i, \downarrow}^\dagger c_{i+\vec{\delta}, \uparrow}^\dagger \right) / \sqrt{2}$, and $\Delta_{i, \delta}^\dagger = \left(c_{i, \uparrow}^\dagger c_{i+\vec{\delta}, \downarrow}^\dagger - c_{i, \downarrow}^\dagger c_{i+\vec{\delta}, \uparrow}^\dagger \right) / \sqrt{2}$. In the presence of the Hubbard U with $U > W$, only $H_W^{(4)}$ should dominate low energy physics. $H_W^{(2)}$ may be neglected since it involves processes containing double occupied sites costing an energy U . $H_W^{(3)}$ describes triplet pair-hopping. The fact that this term comes with a positive sign, and that local triplet configurations are not favored by the superexchange generated by the Hubbard U , gives us arguments to conclude that it will not affect the low energy physics. Thus, $H_W^{(4)}$ is the only relevant term. It may be rewritten as:

$$\begin{aligned} H_W^{(4)} &= 2W \sum_{\vec{i}, \vec{\delta}} \left(\vec{S}_{\vec{i}} \cdot \vec{S}_{i+\vec{\delta}} - \frac{1}{4} (n_{\vec{i}} - 1) (n_{i+\vec{\delta}} - 1) \right) \\ &\quad - \frac{W}{2} \sum_{\vec{i}, \vec{\delta} \neq \vec{\delta}', \sigma} \left(c_{i+\vec{\delta}, \sigma}^\dagger n_{i, -\sigma} c_{i+\vec{\delta}', \sigma} - c_{i+\vec{\delta}, \sigma}^\dagger c_{i, -\sigma}^\dagger c_{i, \sigma} c_{i+\vec{\delta}', -\sigma} \right) \\ &\quad - \frac{W}{2} \sum_{\vec{i}, \vec{\delta} \neq \vec{\delta}', \sigma} \left(c_{i+\vec{\delta}, \sigma}^\dagger (1 - n_{i, -\sigma}) c_{i+\vec{\delta}', \sigma}^\dagger - c_{i+\vec{\delta}, \sigma}^\dagger c_{i, -\sigma}^\dagger c_{i, \sigma}^\dagger c_{i+\vec{\delta}', -\sigma}^\dagger \right) \end{aligned}$$

The first term in the above equation is obtained by setting $\delta = \delta'$ in $H_W^{(4)}$ and corresponds to a superexchange. Here \vec{S}_i denotes the spin operator on site \vec{i} . The second term of the above equation corresponds precisely to the three site term [15]. The third term is just the particle hole transform of the three site term.

The derivation of the relevant terms in H_W via a second order expansion in t/U is along the same line of idea as the above mentioned necessity to include two-particle processes. However, the strong coupling expansion by itself contains neither the physics of flat-band formation nor the unusual properties of the metal-insulator transition. In that sense, the W -term emerges as relevant processes only after complicated many-body processes of the flat-band formation and the second order result provides only a starting point.

In the half-filled case, where QMC simulations are free of the sign-problem, the model (4) has been studied as a function of W/t and at fixed value of the Hubbard repulsion, $U/t = 4$ [14]. It has been found that this model shows a quantum transition at $W_c/t \sim 0.3$ between an antiferromagnetic Mott insulator and $d_{x^2-y^2}$ superconductor. Here, we fix the values of U and W to $U/t = 4$ and $W/t < W_c/t$ and study the model as a function of chemical potential. The organization of the article is the following. In the next section, we study the metal-insulator transition by approaching the critical point from the insulator side. We review the definition of the localization length ξ_l and compute it for the parameter set $U/t = 4$ and $W/t = 0.05$ and show that it diverges as $|\mu - \mu_c|^{-1/2}$. This is the central result of the section and stands in contrast to the $W/t = 0$ results: $\xi_l \sim |\mu - \mu_c|^{-1/4}$. We discuss the relation between the transition in correlation length exponent between $W/t = 0$ and $W/t > 0.05$ in terms of the single-particle density of states. In Sec. (III) we consider finite doping. Here, we are confronted to a sign problem, which makes it exponentially hard to reach *low* temperatures and *large* lattice sizes. We show that at fixed hole density and Hubbard repulsion, the d -wave pair-field correlations increase substantially with growing values of W/t . In contrast no such increase is observed in the extended s -wave channel. We equally study the evolution of $n(\mu)$ as a function of W/t . The last section is devoted to discussions and conclusions.

From the technical point of view, our $T = 0$ data is obtained with the projector QMC (PQMC) algorithm [16,17]. A numerically stable calculation of imaginary time dependent Green functions within this algorithm is described in Ref. [18]. Finite temperature grand canonical QMC algorithms were equally used [19,20]. The generalization of those algorithms to efficiently incorporate the W -term is reviewed in [14]. Dynamical quantities were obtained with the use of the Maximum Entropy method reviewed in [21,22].

II. INSULATOR-METAL TRANSITION AS A FUNCTION OF CHEMICAL POTENTIAL

We start by studying the metal-insulator transition by approaching the critical point from the insulating side. This method has the great advantage that it allows us to avoid the sign problem in the QMC method. This method has already been applied to the case of the single band two-dimensional Hubbard model [7]. There are implicit assumptions in this approach. i) The insulating state, is defined by the vanishing of the Drude weight or charge stiffness, D . The models we consider are particle-hole symmetric at $\mu = 0$ and thus, the critical chemical potential, μ_c , at which the transition occurs is defined by:

$$D(\mu) = 0 \text{ for } |\mu| < \mu_c \quad (10)$$

For the range of chemical potentials for which the Drude weight vanishes, we will assume that the charge susceptibility equally vanishes:

$$\chi_c(\mu) \equiv \frac{\partial n(\mu)}{\partial \mu} = 0 \text{ for } |\mu| < \mu_c. \quad (11)$$

This excludes the possibility of localized states within the charge gap as defined by the vanishing of the Drude weight. The occurrence of localized states within the charge gap could happen in the presence of disorder. ii) Our approach is based on the knowledge of the single-particle Green function. Thus, we have to assume that the quasiparticle gap, $\Delta_{qp} = \lim_{N \rightarrow \infty} E_0^{N+1} - E_0^N$, satisfies:

$$\Delta_{qp} = \mu_c \quad (12)$$

Here, N denotes the number of sites of the considered square lattice and E_0^N is the ground state energy in the N -particle Hilbert space. In the case of an insulator to s-wave superconductor transition, the difference between Δ_{qp} and μ_c is of the order of the superconducting gap at the critical chemical potential. In this case, the insulator-superconductor transition, should be studied with the two-particle Green function. In the case of a transition between an insulator and d -wave superconductor the nodes in the superconducting gap lead to $\Delta_{qp} = \mu_c$. As we will see, in the model of Eq. (4) the d -wave pair-field correlations dominate over the s-wave pair-field correlations at finite doping so that our approach is justified. In the case of a insulator-metal transition where the metallic state is described by a Fermi liquid, the relation $\mu_c = \Delta_{qp}$ clearly holds.

With the above assumptions, the localization length we consider is computed as follows. The zero-temperature Green function, defined by

$$G(\vec{r}, \omega) = i \sum_{\sigma} \int dt e^{i\omega t} \langle \Psi_0 | T c_{\sigma, \vec{r}}(t) c_{\sigma, \vec{0}}^{\dagger}(0) | \Psi_0 \rangle, \text{ with } c_{\sigma, \vec{r}}(t) = e^{iHt} c_{\sigma, \vec{r}} e^{-iHt}, \quad (13)$$

is real for values of $|\omega| < \mu_c$ and satisfies:

$$G(\vec{r}, \omega = \mu) \sim \exp(-|\vec{r}|/\xi_l) \text{ where } \xi_l \sim |\mu - \mu_c|^{-\nu} \quad (14)$$

Here, $|\Psi_0\rangle$ denotes the ground state of the Hamiltonian $H \equiv H_{tUW}$ (see Eq. (4)) at half-band filling. The correlation length exponent ν gives us valuable information on the nature of the insulator-metal transition. ξ_l may be interpreted as the localization length of an impurity state at energy $|\omega| < \mu_c$.

In order to obtain the correlation length exponent, we need an accurate evaluation of the critical chemical potential, as well as the the single-particle Green function $G(\vec{r}, \omega)$ for $|\omega| < \mu$. Both those results may be obtained by using the PQMC algorithm described in [18] to compute the imaginary time single-particle Green function

$$G(\vec{r}, \tau) = \Theta(\tau) \frac{\langle \Psi_0 | \sum_{\sigma} c_{\vec{r}, \sigma}(\tau) c_{\vec{0}, \sigma}^{\dagger} | \Psi_0 \rangle}{\langle \Psi_0 | \Psi_0 \rangle} - \Theta(-\tau) \frac{\langle \Psi_0 | \sum_{\sigma} c_{-\vec{r}, \sigma}^{\dagger}(-\tau) c_{\vec{0}, \sigma} | \Psi_0 \rangle}{\langle \Psi_0 | \Psi_0 \rangle}, \quad (15)$$

where $c_{\vec{r},\sigma}(\tau) = e^{\tau H} c_{\vec{r},\sigma} e^{-\tau H}$. Here, we use the same notation as in Eq. (13) and $\Theta(\tau)$ denotes the Heaviside function. To obtain an estimate of the quasiparticle gap, Δ_{qp} , we fit the tail of $G(\vec{r} = 0, \tau)$ to a single exponential form: $\exp(-\tau\Delta_{qp})$. Alternatively, one may compute Δ_{qp} by fitting the tail of $\sum_{\vec{k}, \epsilon(\vec{k})=0} G(\vec{k}, \tau) / \sum_{\vec{k}, \epsilon(\vec{k})=0} 1$ to the form $\exp(-\tau\Delta_{qp})$. Here, $\epsilon(\vec{k}) = -2t(\cos(k_x) + \cos(k_y))$ and $\epsilon(\vec{k}) = 0$ determines the non-interacting Fermi line in half-filled case. The so obtained values of are presented in Fig. 1 for $W/t = 0, 0.05$ and 0.15 . As argued above, $\mu_c = \Delta_{qp}$ in the model of Eq. (4). From Fig. 1 one notices that size effects become increasingly important as W/t grows.

For $|\omega| < \mu_c$, we can efficiently calculate the single-particle zero-temperature Green function $G(\vec{r}, \omega)$ through the relation

$$G(\vec{r}, \omega) = \int_{-\infty}^{\infty} d\tau G(\vec{r}, \tau) e^{\tau\omega}. \quad (16)$$

The Green function $G(\vec{r}, \tau)$ is computed at half-band filling where the sign problem is not present and the statistical uncertainty does not grow exponentially with lattice size. However, since we are multiplying the QMC data by the factor $e^{\tau\omega}$, the statistical uncertainty will grow exponentially with increasing values of τ for $\tau\omega > 0$. For each lattice size L , we have considered the largest distance $\vec{R} = (L/2, L/2)$. For this distance, $G(\vec{R}, \tau)$ is plotted in Fig. 2. Due to particle-hole symmetry at $\mu = 0$, $G(\vec{R}, \tau) = -G(\vec{R}, -\tau)$.

We carry out the imaginary time integration involved in Eq. (16) in the following way. For *large* positive values of τ , $G(\vec{R}, \tau) \sim \exp(-\tau\Delta_{qp}) \sum_{\sigma} \langle \Psi_0^N | T_{\vec{R}}^{\dagger} c_{\vec{0},\sigma} T_{\vec{R}} | \Psi_0^{N+1} \rangle \langle \Psi_0^{N+1} | c_{\vec{0},\sigma}^{\dagger} | \Psi_0^N \rangle$. Here, $T_{\vec{R}}^{\dagger} c_{\vec{0},\sigma} T_{\vec{R}} = c_{\vec{R},\sigma}$. The Hamiltonian (4) commutes with $T_{\vec{R}}$. Since we are working with periodic boundary conditions, $T_{\vec{R}}^2 \equiv 1$. Thus, $T_{\vec{R}} |\Psi_0\rangle = \pm |\Psi_0\rangle$, and for *large* values of τ , $G(\vec{R}, \tau) \sim \eta G(\vec{0}, \tau)$ with $\eta = \pm 1$. We can fit the tail of $G(\vec{0}, \tau)$ to the form $\alpha \exp(-\tau\Delta_{qp})$ and use this form to estimate the tail of $G(\vec{R}, \tau)$. The advantage lies in the fact that it is easier and more precise to extract the tail from $G(\vec{0}, \tau)$ than from $G(\vec{R}, \tau)$. We now estimate $G(\vec{R}, \omega)$ with

$$G(\vec{R}, \omega) = \int_{-\tau_1}^{\tau_1} d\tau G(\vec{R}, \tau) e^{\tau\omega} + \eta\alpha \int_{\tau_1}^{\infty} d\tau e^{\tau(\omega - \Delta_{qp})} - \eta\alpha \int_{-\infty}^{-\tau_1} d\tau e^{\tau(\omega + \Delta_{qp})}. \quad (17)$$

Clearly, τ_1 has to be chosen large enough such that the left hand side of the above equation is τ_1 independent. Numerically, we choose τ_1 such that for values for $\tau > \tau_1$, $G(\vec{R}, \tau) = \eta G(\vec{0}, \tau)$ within our numerical accuracy.

The so obtained values of $G(\vec{R}, \omega = \mu)$ are plotted in Fig. 3 at $U/t = 4$ and $W/t = 0.05$. for $L = 6$ to $L = 12$ lattices. One may fit the data to the form $\exp(-|\vec{R}|/\xi_l)$ to obtain the localization length ξ_l . The so obtained localization length is plotted versus $|\mu - \mu_c|$ on a log-log scale in Fig. 4. For comparison, we have included our estimate of the localization length at $U/t = 4$ and $W/t = 0$. The central result of this section is the fact that the numerical data are consistent with

$$\begin{aligned} \xi_l &\sim |\mu - \mu_c|^{-1/4} \text{ at } U/t = 4, W/t = 0 \\ \xi_l &\sim |\mu - \mu_c|^{-1/2} \text{ at } U/t = 4, W/t = 0.05 \end{aligned} \quad (18)$$

We also note that the localization length grows at fixed μ with increasing W/t . At $W/t = 0.15$ growing size effects rendered the determination of the localization length difficult for the studied system sizes.

As mentioned in the introduction, the correlation length exponent $\nu = 1/4$ at $W/t = 0$ may be understood in a single-particle picture by the existence of a $|\vec{k}|^4$ dispersion relation around the $(\pm\pi, 0)$ $(0, \pm\pi)$ points in the Brillouin zone. This very flat dispersion relation should lead to a high density of states, $N(\omega) \equiv \frac{1}{N} \sum_{\vec{k}} \text{Im}G(\vec{k}, \omega)$, for frequencies close to the quasiparticle gap. In comparison, at finite values of W/t where we obtain the correlation length exponent $\nu = 1/2$, we expect no anomalous enhancement of $N(\omega)$ at frequencies equal to the quasiparticle gap. In fact, for the generic metal-insulator transition for two-dimensional systems [3], for which one obtains the exponent $\nu = 1/2$, $N(\omega)$ remains a finite constant until it jumps to zero at the band-edge. In order to check this idea, we have computed the one-electron density of states: $N(\omega)$ at half-band filling. At zero-temperature and $\tau t > 0$, $N(\omega)$ is related to the imaginary time QMC data via

$$G(\vec{r} = \vec{0}, \tau) = \frac{1}{\pi} \int_0^\infty d\omega e^{-\tau\omega} N(\omega). \quad (19)$$

$N(\omega)$ is extracted from the above equation with the use of the Maximum-Entropy method. Fig. 5 plots $N(\omega)$ for lattice sizes ranging from $L = 6$ to $L = 16$ at $U/t = 4$ and for both $W/t = 0$ (Figs. 5f to 5j) and $W/t = 0.15$ (Figs. 5a to 5e). Figs. 5k to 5n plots the same data but for $W/t = 0.05$. It is clear that as W/t is enhanced, the large density of states present at $\omega \sim \Delta_{qp}$ vanishes.

III. FINITE DOPING

We now consider finite doping. Here, we are confronted with a sign problem which leads, for a given accuracy, to an exponential increase of CPU time as the lattice size and inverse temperature grows.

We first consider the particle number as a function of chemical potential at $U/t = 4$ for $W/t = 0, W/t = 0.05$ and $W/t = 0.15$ on an 8×8 lattice in a temperature window $T = 0.5t$ to $T = 0.2t$. The data is plotted in Fig. (6). Finite size effects grow as a function of W/t . This may be seen for example in Fig. 1 where it becomes increasingly hard to extrapolate to the thermodynamic limit for *large* values of W/t . To give the reader a feeling of the size effects involved, we have plotted at $W/t = 0.15$ and $T = 0.25t$, some data for an $L = 10$ lattice (see Fig. 6) For the discussion of the data, we will omit the size effects in the considered temperature range. The dashed lines correspond to the value of the quasiparticle gap obtained in the zero-temperature and thermodynamic limits. (see Fig.1). As discussed above, we expect for our model $\Delta_{qp} = \mu_c$. Hence, at $T = 0$, $n(\mu) = 1$ for $\mu > \mu_c$ and $n(\mu) < 1$ for $\mu < \mu_c$. From this construction, one may see that temperature effects are much more pronounced at $W/t = 0$ than at $W/t = 0.15$. This result is easily understood within a single-particle picture mentioned in the introduction. The flatness of the dispersion relation signaled by the correlation length exponent $\nu = 1/4$ at $W/t = 0$ leads to large temperature effects in $n(\mu)$. The transition to the description of the insulator-metal transition with exponent $\nu = 1/2$, leads to the suppression of large temperature effects in $n(\mu)$. At $W/t = 0$ it was possible to pin down the exponent of the charge susceptibility, $\chi_c \sim |\mu - \mu_c|^{-1/2}$ only with the use of zero-temperature algorithms such as the PQMC [4,5] . As argued above, at finite values of W , temperature effects are reduced. Nevertheless, it is still difficult to pin down the charge susceptibility exponent from finite temperature data.

We conclude this section by giving some numerical evidence, that the cause of the transition in the nature of the insulator-metal transition is related to the enhancement of $d_{x^2-y^2}$ pairing correlations in the metallic state. The vertex contribution to the equal time pair-field correlations is given by:

$$P_{d,s}^v(\vec{r}) = P_{d,s}(\vec{r}) - \sum_{\sigma, \vec{\delta}, \vec{\delta}'} f_{d,s}(\vec{\delta}) f_{d,s}(\vec{\delta}') \left(\langle c_{\vec{r},\sigma}^\dagger c_{\vec{\delta}',\sigma} \rangle \langle c_{\vec{r}+\vec{\delta},-\sigma}^\dagger c_{\vec{0},-\sigma} \rangle + \langle c_{\vec{r},\sigma}^\dagger c_{\vec{0},\sigma} \rangle \langle c_{\vec{r}+\vec{\delta},-\sigma}^\dagger c_{\vec{\delta}',-\sigma} \rangle \right) \quad (20)$$

where

$$P_{d,s}(\vec{r}) = \langle \Delta_{d,s}^\dagger(\vec{r}) \Delta_{d,s}(\vec{0}) \rangle \quad (21)$$

with

$$\Delta_{d,s}^\dagger(\vec{r}) = \sum_{\sigma, \vec{\delta}} f_{d,s}(\vec{\delta}) \sigma c_{\vec{r},\sigma}^\dagger c_{\vec{r}+\vec{\delta},-\sigma}^\dagger. \quad (22)$$

Here, $f_s(\vec{\delta}) = 1$ and $f_d(\vec{\delta}) = 1(-1)$ for $\vec{\delta} = \pm \vec{a}_x$ ($\pm \vec{a}_y$). Per definition, $P_{d,s}^v(\vec{r}) \equiv 0$ in the absence of interactions. Fig. 7 plots $P_{d,s}^v(L/2, L/2)$ at $\langle n \rangle = 0.78$, and $U/t = 4$ as a function of temperature. We consider an 8×8 lattice with $W/t = 0$, $W/t = 0.05$ and $W/t = 0.15$. As W/t grows, there is a substantial increase in $P_{d,s}^v(L/2, L/2)$. This stands in contrast to the signal obtained in the extended s -wave channel where virtually no enhancement as a function of W/t is seen.

IV. DISCUSSION AND CONCLUSIONS

We have given numerical evidence showing that the nature of the metal insulator transition in the two-dimensional Hubbard model is radically altered by the inclusion of the W -term. The low energy physics contained in this term was argued to be described by the three site terms obtained in a strong coupling expansion of the Hubbard model. The presented data support the interpretation that the change in the nature of the doping induced metal insulator transition as a function of W/t is related to the onset of d -wave superconductivity in the metallic state at finite W/t . The critical value of W , W_c^μ/t , at which the nature of the metal-insulator transition changes is uncertain. We can at present only give an upper-bound: $W_c^\mu/t < 0.05$ for $U/t = 4$.

Our result are best described under the assumption of hyperscaling [1,2] where it is postulated that the singular part of the free energy scales as $f_s(\Delta) = \Delta^{\nu(d+z)}$ and that there is a single relevant length scale ξ . Here, $\Delta \equiv |\mu - \mu_c|$ is related to the length $\xi \sim \Delta^{-\nu}$, d is the dimensionality and z the dynamical exponent. Under the above assumptions, the charge susceptibility χ_c , charge stiffness D , and localization length ξ_l , satisfy:

$$\xi_l \sim \Delta^{-\nu}, \quad \chi_c \sim \Delta^{\nu(d-z)}, \quad D \sim \Delta^{\nu(d+z-2)}, \quad (23)$$

Since the control parameter, Δ , corresponds to the chemical potential, one obtains the additional constraint $\nu z = 1$ as well as $\delta \sim \Delta^{\nu(d+z)-1}$, δ being the doping concentration.

Thus, in the case of a doping induced metal-insulator transition, there is only one free parameter. The generic band metal-insulator transition does satisfy the above assumption and belongs to the $z = 2$, $\nu = 1/2$ universality class. We also note that the doping induced metal-superfluid transition for two-dimensional bosons, is described by hyperscaling with exponents: $\nu = 1/2$ and $z = 2$ [23]. For the two-dimensional Hubbard model at $U/t = 4$, we have two numerical results, the localization length as well as the charge susceptibility, which are consistent with the above scaling relations provided that $\nu = 1/4$ and $z = 4$. At $W/t = 0.05$ and $U/t = 4$, our results for the localization length, $\xi_l \sim |\mu - \mu_c|^{-1/2}$ imply that $\nu = 1/2$. Furthermore, from our finite temperature results for $n(\mu)$, it is plausible to assume that $\chi_c \sim |\mu - \mu_c|^0$ in the zero-temperature and thermodynamic limits as would be expected if the hyperscaling assumption is satisfied. For the confirmation the hyperscaling assumption, the calculation of the charge stiffness at $T = 0$ as a function of doping and W/t is crucial. The prediction that $D \sim \delta^2$ at $W = 0$ and that $D \sim \delta$ at $W > W_c^\mu$ remains for further studies.

The above analysis suggests that the metal-insulator transition characterized by the dynamical exponent $z = 4$ is destabilized by a finite value of W to the superconductor-insulator transition with $z = 2$. When the dynamical exponent z changes from $z = 4$ to $z = 2$ by inclusion of a finite amplitude of the W -term, the thus obtained wider dispersion relation causes a strong kinetic energy gain. This may be the origin of the instability of the incoherent metals with $z = 4$ to the superconducting state with $z = 2$. A flat band structure itself could be mimicked by a simple modification of the original band structure (e.g the inclusion of next-nearest neighbor transfer). However, to understand the instability due to the change in the universality class and the origin of the release of the suppressed coherence (i.e. $D \sim \delta^2$), it is crucial to notice that the $z = 4$ metals are a consequence of strong correlation effects and have to be constructed not from simple band electrons but from strongly renormalized charge excitations around the $(\pm\pi, 0)$ and $(0, \pm\pi)$ points in the Brillouin zone [2,24].

We have previously shown that at $T = 0$, $\langle n \rangle = 1$, and $U/t = 4$, W drives the system from an antiferromagnetic Mott insulator to a $d_{x^2-y^2}$ superconductor. This quantum transition occurs at $W_c/t \sim 0.3$. In the superconducting state at half-band filling, charge and spin degrees of freedom have been studied and show rich physics [14]. The data shows the extreme compatibility between antiferromagnetic fluctuations and d -wave superconductivity. The relation between this state and the state obtained by doping the antiferromagnetic Mott insulator at $U/t = 4$, $W_c^\mu < W < W_c$ is intriguing. High- T_c cuprates are obtained by doping the Mott insulator. Some aspects of the experimental data seem to show the remnant of extreme compatibility between magnetism and d -wave superconductivity. In nuclear magnetic resonance studies of $YBa_2Cu_4O_8$ and $HgBa_2Ca_2Cu_3O_{8+\delta}$, T_{2G} of Cu -sites, which measures predominantly $\text{Re}\chi(\vec{q} = (\pi, \pi), \omega = 0)$ continues to grow monotonically with decreasing temperature even below the temperature scale at which $1/T_1T$ starts decreasing [25]. Although this feature is not clear cut in the single-layer-type mercury compounds [26] the tendency of stronger growth of $1/T_{2G}$ than $1/T_1T$ above T_c seems to be universal. An extreme case of this feature is seen in our numerical calculations in the superconducting state at $\langle n \rangle = 1$ where in the low temperature limit, $1/T_1T$ scales to zero while $\text{Re}\chi(\vec{q} = (\pi, \pi), \omega = 0)$ diverges. The most remarkable feature is that the dynamical spin structure factor, $S(\vec{q}, \omega)$, at $\vec{q} = (\pi, \pi)$ has a peak structure with diverging weight at finite frequencies [14]. In

$La_{2-x}Sr_xCuO_4$, $S(\vec{q}, \omega)$, below T_c shows a sharp peak in momentum space centered at the incommensurate wave-vector, $\vec{Q}_\delta = (\pi, \pi) + \delta(\pi, 0)$ and at relatively high energies: $\omega > 7meV$ [27]. This indicates that, the magnetic length scale at relatively high energies becomes large ($> 50\text{\AA}$) as the temperature is lowered below T_c . In $YBa_2Cu_3O_{7-x}$, a sharp peak in frequency at $30 - 40 meV$ is observed in the superconducting phase [28,29]. These features again share some similarity with the $t - U - W$ model at $\langle n \rangle = 1$ in the superconducting state. At temperatures below the Kosterlitz-Thouless transition, spectral weight in $S(\vec{q}, \omega)$ is transferred from low frequencies to higher frequencies. In the low temperature limit, $S(\vec{q} = (\pi, \pi), \omega)$ shows a sharp peak in momentum space at finite frequencies. This peak is associated with the coherent part of the spin response since it is related to the long distance power-law decay of the equal time spin-spin correlations [14].

In conclusion, the $t - U - W$ model at finite values of W/t appears to be a promising minimal model for high- T_c superconductors. Clearly, further studies for the complete understanding of physical properties of the model as function of W , doping and temperature are required.

We thank D.J. Scalapino for many stimulating discussions as well as H. Tsunetsugu and A. Muramatsu. The numerical calculations were carried out on the FACOM VPP500 at the Supercomputer Center of the Institute for Solid State Physics, Univ. of Tokyo. This work was financially supported by a Grant-in-Aid for ‘Research for the Future’ program under the project number JSPS-RFTF97P01103, by a Japan-Germany joint research project from the Japan Society for the Promotion of Science as well as by a Grant-in-Aid for Scientific Research on the Priority Area ‘Anomalous Metallic State near the Mott Transition’ from the Ministry of Education Science and Culture Japan. F.F.A. thanks the Swiss National Science foundation for partial financial support under the grant number 8220-042824.

REFERENCES

- [1] M. Imada, J. Phys. Soc. of Jpn. **64**, 2954 (1995).
- [2] M. Imada, A. Fujimori and Y. Tokura. Metal-Insulator Transitions, to be published in Rev. Mod. Phys.
- [3] Our working definition of the generic band metal-insulator transition is the one realized for free fermions, $H_0 = \sum_{\vec{k},\sigma} \frac{\vec{k}^2}{2m} c_{\vec{k},\sigma}^\dagger c_{\vec{k},\sigma}$ at zero chemical potential $\mu = 0$.
- [4] N. Furukawa and M. Imada, J. Phys. Soc. Jpn. **62**, 2557, (1993).
- [5] M. Kohno, Phys. Rev. B **55**, 1435, (1997).
- [6] J. Jaklic and P. Prelovsek, Phys. Rev. Lett. **77**, 892, (1996).
- [7] F.F. Assaad and M. Imada, Phys. Rev. Lett. **76**, 3176, (1996).
- [8] F.F. Assaad and M. Imada, Phys. Rev. Lett. **74**, 3872, (1995).
- [9] Z.-X. Shen and J. R. Schrieffer, Phys. Rev. Lett. **78**, 1771, (1997).
- [10] In the presence of long-range antiferromagnetic order, the vector (π, π) belongs to the reciprocal lattice since the Brillouin has been folded. Growing antiferromagnetic correlations will give some precursor of this Umklapp scattering.
- [11] K. Gofron, et al. Phys. Rev. Lett. **73**, 3320, (1994).
- [12] D.S. Dessau et al. Phys. Rev. Lett. **71**, 2781, (1993). Z.-X. Shen and D.S. Dessau, Phys. Rep. **253**, 1, (1995).
- [13] The flat bands observed experimentally, are much flatter than the usual Van-Hove singularity. In Ref. [11] it has been argued that they yield a powerlaw singularity in the density of states.
- [14] F.F. Assaad, M. Imada and D.J. Scalapino, Phys. Rev. Lett. **77**, 4592, (1996). Phys. Rev. B, in press.
- [15] J.E. Hirsch, Phys. Rev. Lett **54**, 1317, (1985).
- [16] G. Sugiyama and S.E. Koonin, Annals of Phys. **168** (1986) 1.
- [17] S. Sorella, S. Baroni, R. Car, And M. Parrinello, Europhys. Lett. **8** (1989) 663. S. Sorella, E. Tosatti, S. Baroni, R. Car, and M. Parinello, Int. J. Mod. Phys. B **1** (1989) 993.
- [18] F.F. Assaad and M. Imada, J. Phys. Soc. Jpn. **65**, 189, (1996).
- [19] J.E. Hirsch, Phys. Rev. B **31**, 4403, (1985).
- [20] S.R. White et al. Phys. Rev. B **40**, 506, (1989).
- [21] M. Jarrel and J.E. Gubernatis, Physics Reports, **269**, (1996) 133
- [22] W. von der Linden, Applied Physics A **60**, (1995), 155.
- [23] M.P.A. Fisher, P.B. Weichman, G. Grinstein and D.S. Fisher: Phys. Rev. B **40** (1989) 546.
- [24] M. Imada, In Computer Simulation Studies in Condensed matter Physics X, ed. by D.P. Landau et al. (Springer Verlag, Heidelberg, Berlin, 1997).
- [25] Y. Itoh et al. Y. Itoh, H. Yasuoka, Y. Fujiwara, Y. Ueda, T. Machi, I. Tomeno, K. Tai, N. Koshizuka and S. Tanaka, J. Phys. Soc. Jpn., **61**, 1287, (1992). M.H. Julien et al. Phys. Rev. Lett **76**, 4238, (1996).
- [26] Y. Itoh et al. preprint.
- [27] T.E. Mason, A. Schröder, G. Aeppli, H.A. Mook, and S.M. Hayden, Phys. Rev. Lett. **77**, 1604, (1996).
- [28] J. Rossat-Mignod et al. Physica (Amsterdam) **185C - 189C**, 86, (1991).
- [29] H.F. Fong et al. Phys. Rev. Lett. **75**, 316, (1995). H.F. Fong et al. Phys. Rev. Lett. **78**, 713, (1997).

FIGURES

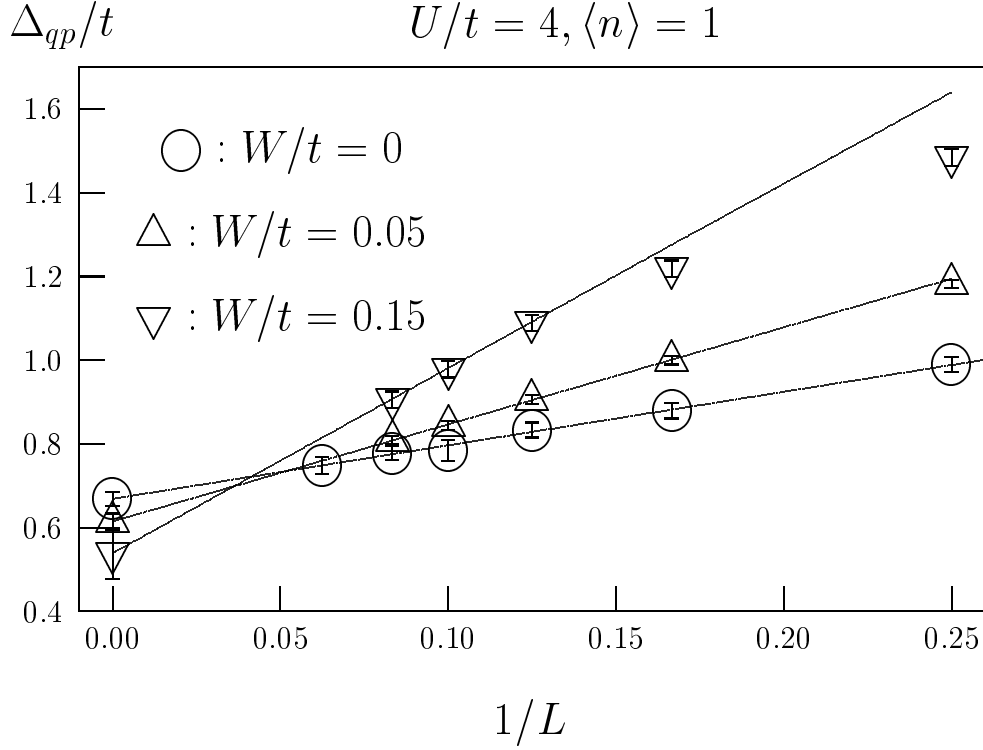


FIG. 1. The quasiparticle gap $\Delta_{qp} = E_0^{N+1} - E_0^N$ as a function of inverse linear lattice length L at $U/t = 4$ and three values of W/t . Here, $N = L^2$. The solid lines correspond to least square fits to the form $a + b/L$. The data points at $1/L = 0$, are the so extrapolated values of the quasiparticle gap. At $W/t = 0.15$ the lattice sizes $L = 12, 10$ and 8 were taken into account for the fit.

$$|G(\vec{r} = (L/2, L/2), \tau)|$$

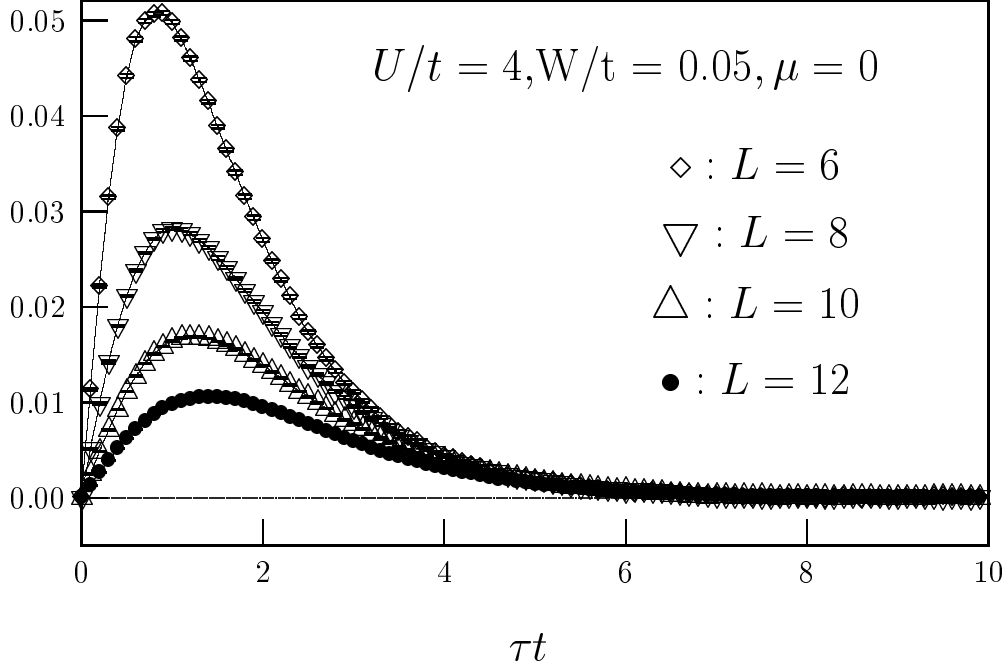


FIG. 2. The single particle Green function at half-filling $\vec{R} = (L/2, L/2)$, $U/t = 4$, $W/t = 0.05$ as a function of imaginary time τ . Due to particle-hole symmetry, and the fact that the considered values of L are even, $G(\vec{R}, -\tau) = -G(\vec{R}, \tau)$. It is interesting to compare this data to the case $W/t = 0$ ([7]). At $W/t = 0.05$, an added electron propagates quicker in imaginary time than at $W/t = 0$.

$$U/t = 4, W/t = 0.05, \langle n \rangle = 1$$

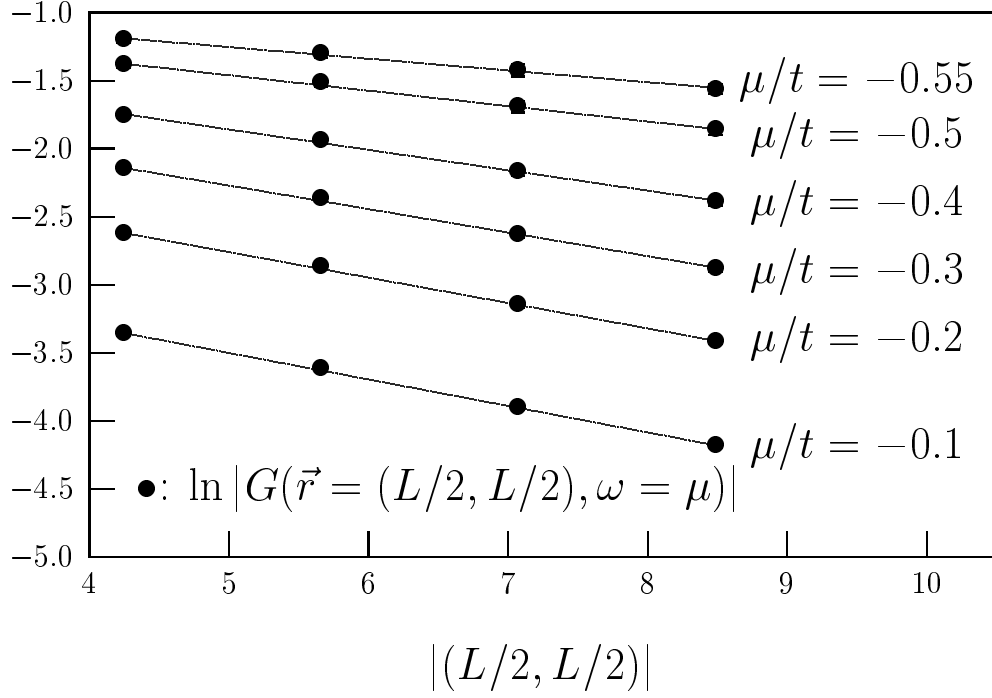


FIG. 3. $G(\vec{R} = (L/2, L/2), \omega)$ as obtained from equation 16 as a function of L . Here we consider the parameter set $U/t = 4, W/t = 0.05$ values of ω satisfying $\omega < \Delta_{qp} \sim 0.62t$. The solid lines are least square fits to the form $a \exp(-L/\sqrt{2}\xi_l)$.

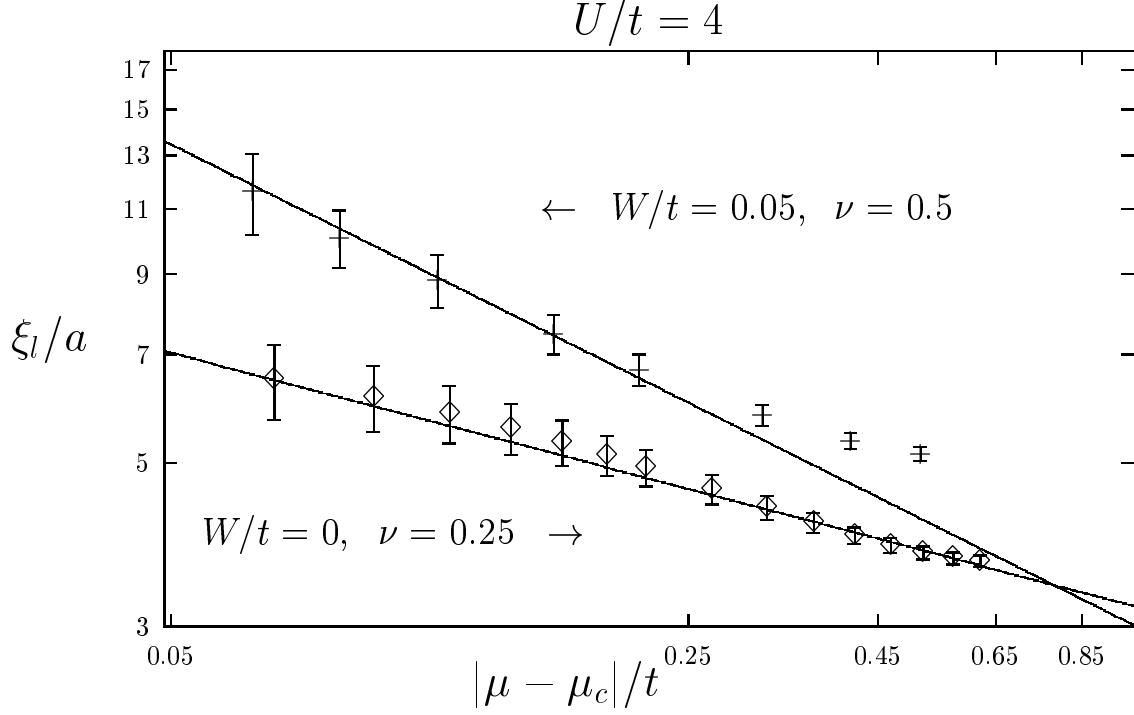
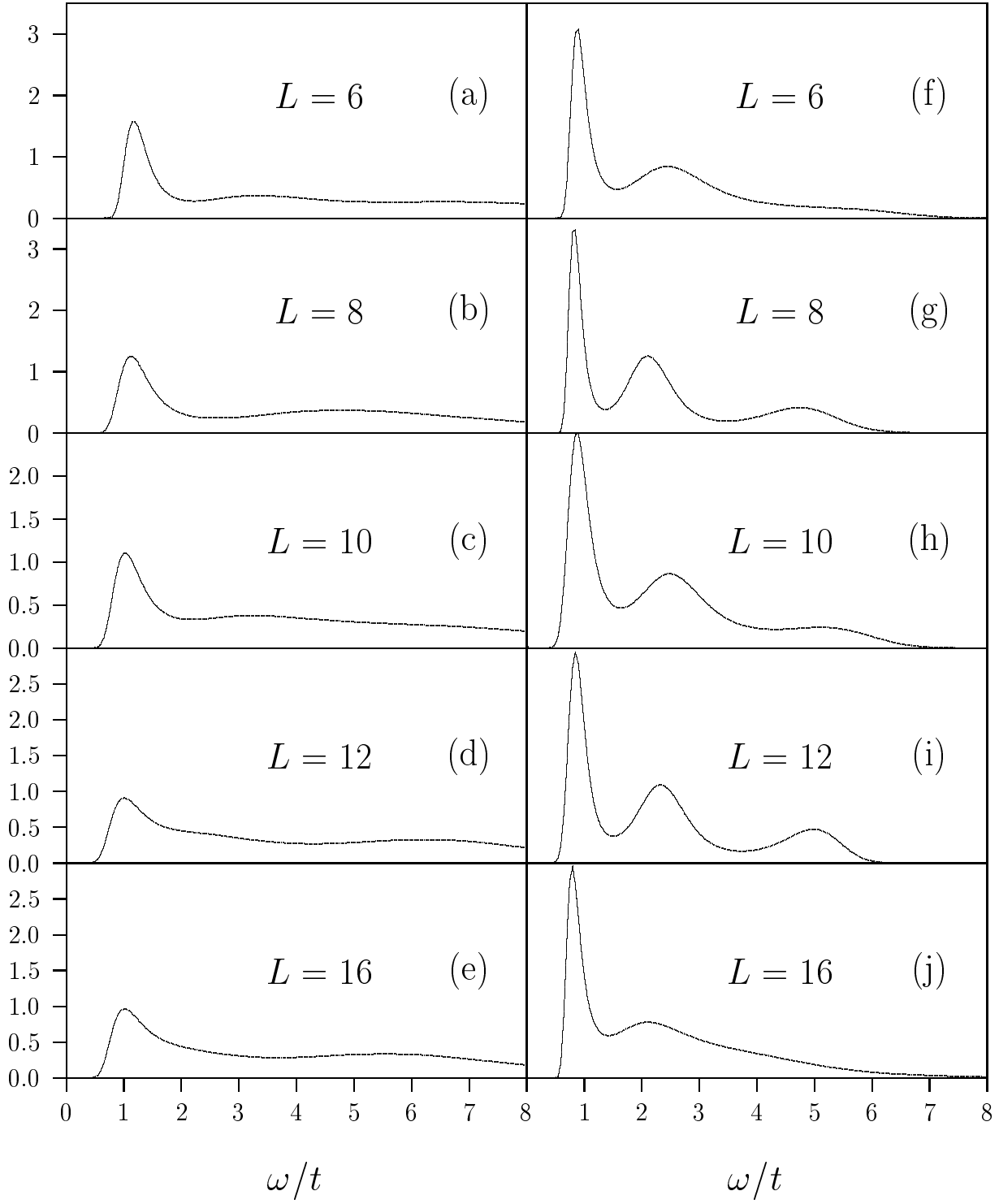


FIG. 4. The localization length as a function of $|\mu - \mu_c|$. The data at $W/t = 0, U/t = 4$ is reproduced from Ref. [7]. The data at $W/t = 0.05, U/t = 4$ is obtained from Fig. (3). The solid lines correspond to the form $|\mu - \mu_c|^{-\nu}$ for $\nu = 0.5$ and $\nu = 0.25$. The data is consistent with $|\mu - \mu_c|^{-1/2}$ at $W/t = 0.05$ and $|\mu - \mu_c|^{-1/4}$ at $W/t = 0$.

$$N(\omega), U/t = 4, \langle n \rangle = 1, T = 0$$

$$W/t = 0.15 \qquad W/t = 0.0$$



$$N(\omega), U/t = 4, \langle n \rangle = 1, T = 0$$

$$W/t = 0.05$$

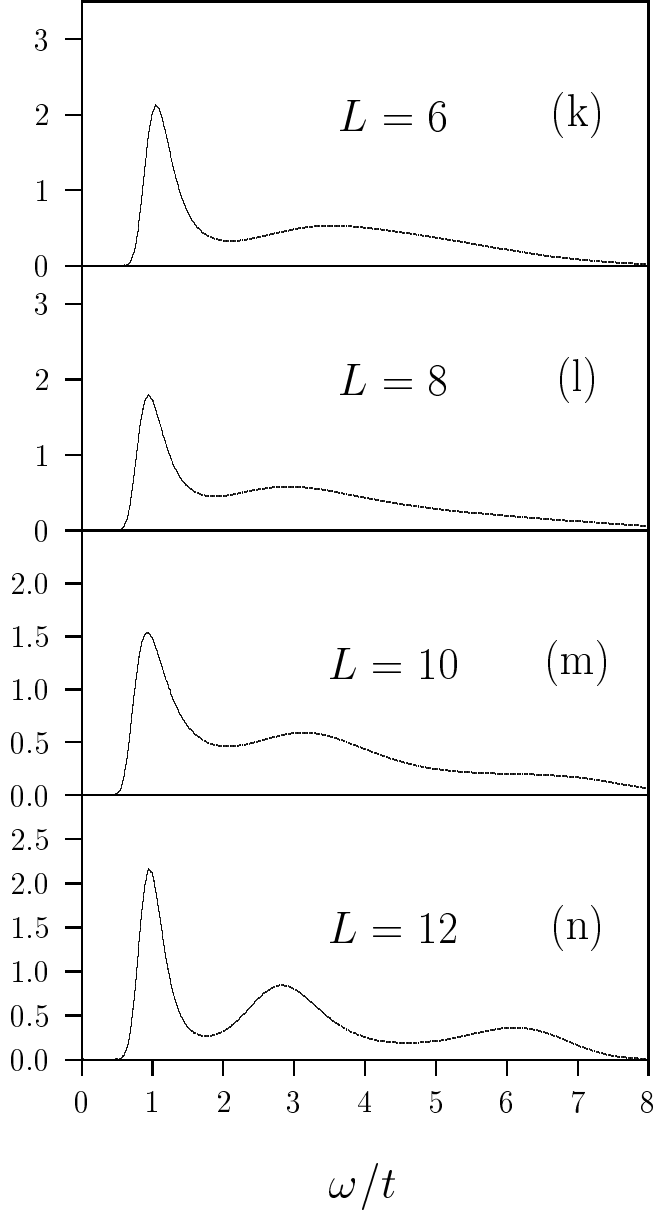


FIG. 5. $T = 0$ density of states, $N(\omega)$ at half-band filling (i.e. $\mu = 0$) for $U/t = 4$ and (a) to (e) $W/t = 0.15$, (f) to (j) $W/t = 0$ and (k) to (n) $W/t = 0.05$.

$$U/t = 4, L = 8$$

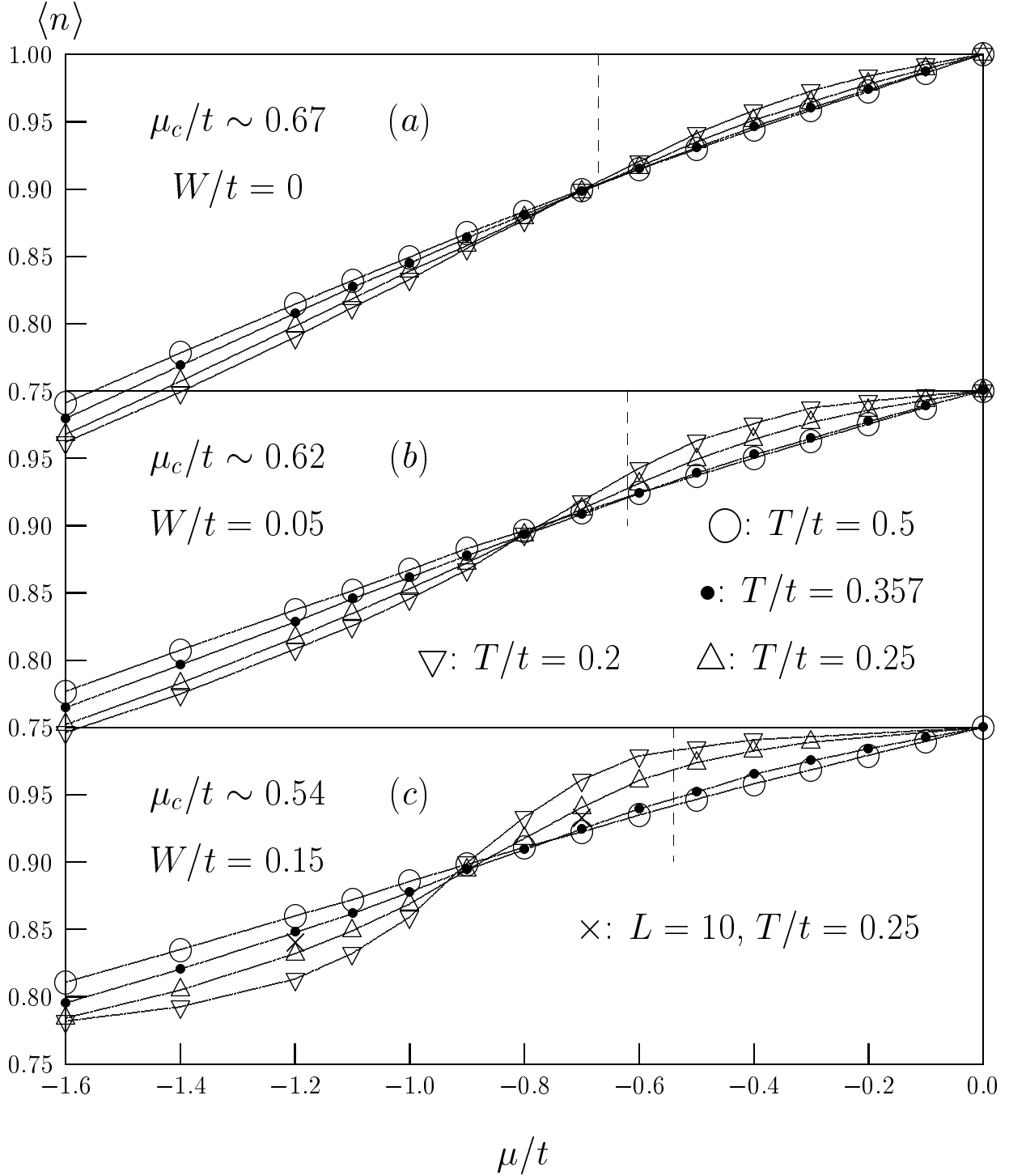


FIG. 6. Number of particles per site, n , as a function of chemical potential for temperatures ranging from $T = 0.2t$ to $T = 0.5t$. The dashed vertical line corresponds to the quasiparticle gap at $T = 0$ and in the thermodynamic limit. This data is obtained from Fig. 1. We consider an 8×8 lattice, $U/t = 4$ and (a) $W/t = 0$, (b) $W/t = 0.05$ and (c) $W/t = 0.15$. In Fig. (c) we have included some data points for a 10×10 lattice.

$$U/t = 4, \langle n \rangle = 0.78, L = 8$$

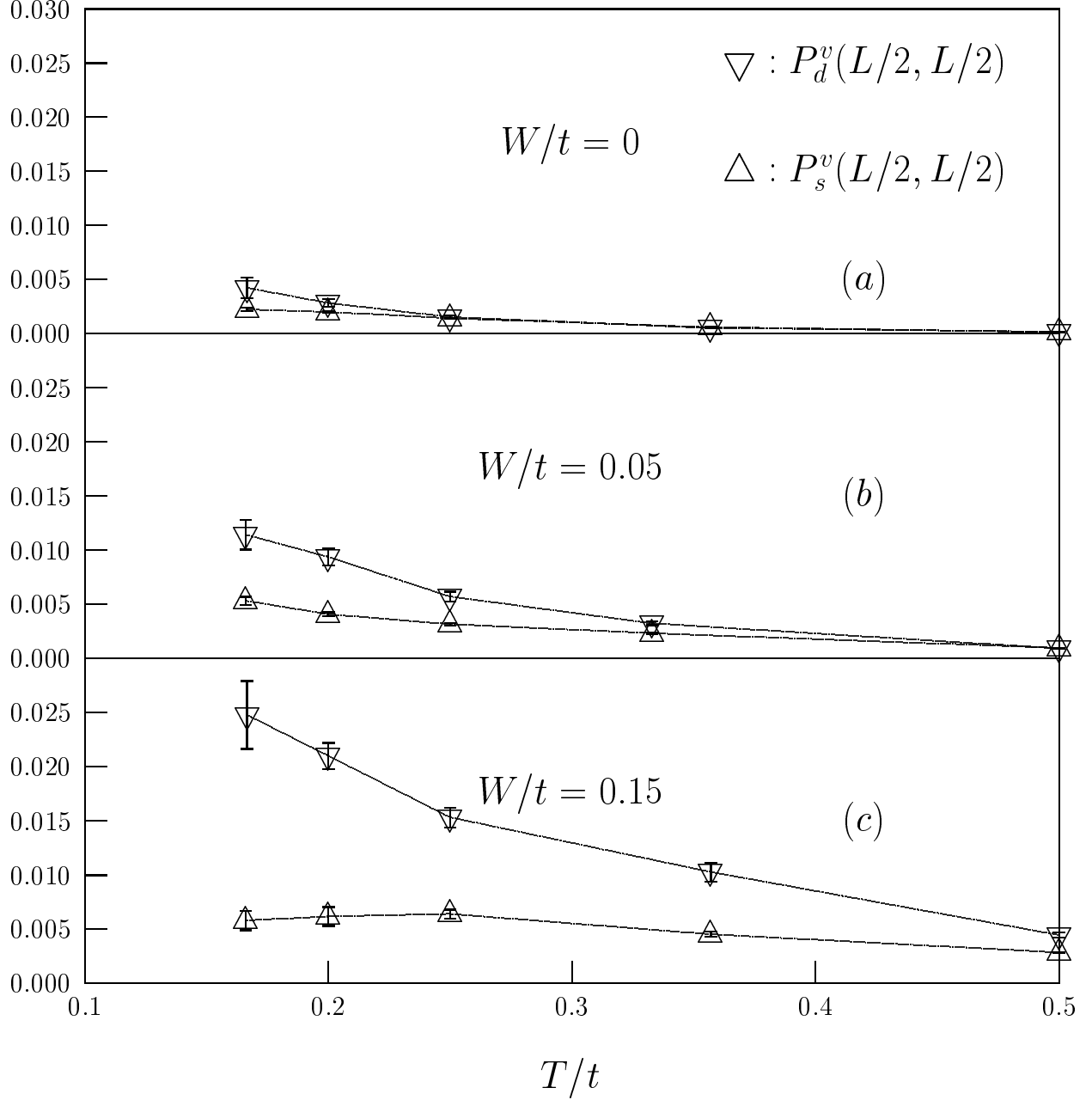


FIG. 7. Vertex contribution to the pair-field correlations at the largest distance on an $L = 8$ lattice in both the d -wave and extended s -wave channel. The data is plotted versus temperature. Here we fix the the particle number to $\langle n \rangle = 0.78$, the Hubbard repulsion to $U/t = 4$ and consider (a) $W/t = 0$, (b) $W/t = 0.05$ and (c) $W/t = 0.15$